Tritium distribution analysis of Be limiter tiles from JET-ITER þÿlike wall campaigns using imaging plate technique and þÿ²-ray induced X-ray spectrometry

JET Contributors

2020-11

JET Contributors , Lee , S E , Likonen , J & Helariutta , K 2020 , ' Tritium distribution analysis of Be limiter tiles from JET-ITER like wall campaigns using imaging plate technique and þÿ²-ray induced X-ray spectrometry ' , Fusion Engineering and Design , v

http://hdl.handle.net/10138/347661
https://doi.org/10.1016/j.fusengdes.2020.111959

Tritium Distribution Analysis of Be Limiter Tiles from JET-ITER Like Wall Campaigns using Imaging Plate Technique and β-ray Induced X-ray Spectrometry

S. E. Lee[a*], Y. Hatano[a], M. Hara[a], S. Masuzaki[b], M. Tokitani[b], M. Oyaizu[c], H. Kurotaki[c], D. Hamaguchi[c], H. Nakamura[c], N. Asakura[c], Y. Oya[d], J. Likonen[e], A. Widdowson[f], S. Jachmich[g], K. Helariutta[h], M. Rubel[i] and JET contributors[†]

[a]*University of Toyama, Toyama 930-8555, Japan*
[b]*National Institute for Fusion Science, Oroshi 322-6, Toki 509-5292, Japan*
[c]*National Institutes for Quantum and Radiological Science and Technology (QST), Rokkasho Aomori 039-3212, Japan*
[d]*Shizuoka University, Shizuoka, 422-8529, Japan*
[e]*VTT Technical Research Centre of Finland, P.O.Box 1000, FI-02044 VTT, Finland*
[f]*Culham Centre for Fusion Energy, Culham Science Centre, Abingdon, OX 14 3DB, UK*
[g]*Association Euratom-Etat Belge, ERM-KMS, Brussels Belgium*
[h]*University of Helsinki, P.O. Box 55, FI-00014 University of Helsinki, Finland*
[i]*KTH Royal Institute of Technology, 100 44 Stockholm, Sweden*
[†]*See appendix to paper of X. Litaudon, Nucl. Fusion 57 (2017) 102001*

Abstract

Tritium (T) distribution on the plasma-facing surfaces (PFSs) and inside castellation of Be limiter tiles from the JET tokamak with the ITER-like wall (ILW) was analyzed using imaging plate (IP) technique and β-ray induced X-ray spectrometry (BIXS). Regarding to PFSs, the outer poloidal limiter (OPL) showed significantly higher T concentrations than the inner wall guard limiter (IWGL) and upper dump plate (DP). The concentration of T on OPL was high at the central part. However, deuterium (D) and metallic impurities showed maximum concentration at the edges. This difference in distributions indicated different deposition and retention mechanisms between T and D. In contrast, deposition profiles of T concentrations on the castellated surfaces extended up to ~ 5 mm into the gap, i.e. were similar to those of D and metallic impurities found by ion beam analysis.

Keywords: tritium analysis, beryllium, radiography, Joint European Torus, ITER-like wall

1. Introduction

The Joint European Torus (JET) has been operated since year 2011 with the ITER-like wall (ILW): beryllium (Be) limiter tiles in the main chamber and bulk tungsten (W) and tungsten-coated carbon-fiber composite (W-CFC) tiles in the divertor. The JET-ILW discharges were mainly fueled by deuterium (D) in three consecutive campaigns performed in 2011-2012 (ILW-1), 2013-2014 (ILW-2) and 2015-2016 (ILW-3) [1,2].

Understanding of fuel retention mechanisms in a fusion device with Be and W walls is important for safety assessment in future fusion devices including ITER. From this viewpoint, distribution of D has been examined through post-mortem analyses of retrieved tiles using various techniques including ion beam analysis (IBA) [2-4], secondary ion mass spectroscopy (SIMS) [5] and thermal desorption spectrometry (TDS) [4,6]. These measurements showed that fuel retention with ILW was far smaller than that with carbon wall [7], and the main retention mechanism was co-deposition with Be and other impurities. In the divertor region, high D concentration was observed at the inboard side where thick Be deposition was formed [3,5]. The analysis of outer poloidal limiter (OPL) in the main chamber showed high D concentration at the edges in toroidal direction [2-4] where high concentrations of metallic impurities were observed [1-3,8]. Rubel et al. [9] have examined D distributions in castellation grooves of the Be limiter tiles and found graded D concentration profiles

extended to ~ 1-3 mm from the entrance to the gap.

Regarding to tritium (T) produced by DD fusion reactions ($^2D + {}^2D \rightarrow {}^3T$ [1.01 MeV] + ^1p [4.04 MeV]), its distribution on the retrieved tiles was examined using imaging plate (IP) technique [10], β-ray induced X-ray spectrometry (BIXS) [11], TDS [4,12,13] and dissolution method [12,13]. The distribution of T in the divertor region was more or less similar to that of D; the high T concentration was observed at the inboard region with Be deposition layers [10]. This observation indicates a part of T was thermalized in the plasma and co-deposited with D, though implantation of high energy T was also confirmed using BIXS measurements in the upper part of divertor region [11]. The distributions of T on the Be tiles retrieved from the main chamber after ILW-1 and ILW-2 have been examined by Pajuste et al. [12,13] by measuring T retention in selected castellation samples cut from Be tiles. The method based on dissolution in acid and TDS were used. The reported T concentration on OPL was higher than that on inner wall guard limiter (IWGL) and dump plate (DP) at the top of the main chamber [12,13]. The highest T concentration was found at the central part of OPL [13], though D showed the highest concentration at the edges of this tile [2-4]. The mechanisms underlying this difference has not been fully understood. The T distribution in castellation grooves has not been examined.

In this study, Be tiles retrieved after ILW-1 were analyzed by the imaging plate IP technique (radiography) and beta-ray induced X-ray spectrometry BIXS. The T distributions on plasma-facing surfaces (PFSs) and on surfaces inside the castellated grooves were examined using IP technique. The implantation depth of T was evaluated using BIXS and Monte Carlo simulation toolkit Geant4 [14-17]. The tiles exposed to the plasma in ILW-3 and all three campaigns (ILW-1,2,3) were also analyzed for comparison.

2. Experimental

Castellated samples were cut from selected positions of mid-plane IWGL, mid-plane OPL and DP tiles retrieved after ILW-1. The locations of the tiles in the JET vacuum vessels are shown in Fig. 1, and the positions from where the samples were taken are indicated in Fig. 2. Those samples were shipped to the International Fusion Energy Research Center (IFERC), National Institutes for Quantum and Radiological Science and Technology (QST) in Rokkasho, Japan. For the IP measurement, β-ray sensitive imaging plate (BAS IP TR, GE Healthcare Japan) was used. The examined surfaces were in contact with IP sheets for 18-27 h in the dark, and then 2-dimensional distributions of photo-stimulated luminescence (PSL) from IP sheets were obtained using a laser scanner (FLA-7000, Fujifilm). Plastic plates labelled with known amounts of T (American Radiolabeled Chemicals, ART0123A) were used as reference samples for quantitative analysis. BIXS measurements were performed for PFSs under argon (Ar) gas atmosphere with a silicon drift detector (SDD) with 8 μm-thick Be window (X-123SDD, Amptek Inc.). The Be window of SDD has negligible transmittance to X-rays below 0.6 keV [18] and characteristic X-rays of Be (0.109 keV) cannot be detected in the X-ray spectra.

IWGL, OPL and DP exposed to the plasma in ILW-3, and IWGL and OPL installed in the JET for all three ILW campaigns (ILW-1,2,3) were also subjected to IP measurements in VTT Technical Research Centre of Finland. In this case, IP sheets were covered with 1.2 or 2.0 μm thickness polyphenylene sulfide (PPS) films to avoid contamination by T and Be. After exposure to β-rays from the tiles for 16-19 h in the dark, 2-dimensional PSL distributions were obtained by analyzing IP sheets at the University of Helsinki using a laser scanner (FLA-5100, Fujifilm).

The tiles used for post-mortem analysis in this paper are summarized in Table 1. Tile codes are also given in this table. The operation parameters of ILW campaigns are shown in Table 2. Input energy in ILW-3 was larger than that in ILW-1, limiter plasma time in the former was shorter than that in the

latter.

3. Results and discussions

3.1 Plasma-facing surfaces

Fig. 2 shows IP images of PFSs of the Be limiter tiles exposed to plasma in ILW-1, ILW-3 and ILW-1,2,3 together with the photos of tiles. The numbers indicate positions of castellation samples. A color scale from blue to red indicates the PSL intensity from the lowest to the highest; regions with red color suggest enrichment of T. As described earlier, the measurements in VTT were performed after wrapping the tiles with 1.2 μm or 2.0 μm-thick PPS films which attenuate intensity of β-rays by a factor of 12 and 40, respectively. The contrast in IP images in Fig. 2 was obtained after correction for this attenuation effects by the PPS films. For IWGL and OPL retrieved after ILW-3, the upper regions of PFSs with width of about 20 mm were covered by IP, while whole PFSs were analyzed for ILW-1,2,3 tiles. Green-blue contrasts indicated by black arrows in the images of IWGL and DP are artifacts due to static electricity induced at removal of the thin PPS films.

As shown in Fig. 2, the T distribution on IWGL and DP were more or less uniform after ILW-1, ILW-2 and ILW-1,2,3. In contrast, the distribution of T on OPL was clearly inhomogeneous in toroidal direction for all three cases, and the highest concentration was detected at the center of tile. The T retention at the central part of OPL after ILW-1 (sample 127) was evaluated to be 80 kBq/cm^2 by assuming that T implantation depth was 6 μm (see BIXS result in Fig. 5 (b)). The density of sample was presumed to be 1.85 g/cm^3. Line profiles of T along toroidal direction on the PFSs of OPL exposed to plasma in ILW-3 and ILW-1,2,3 are plotted in Fig. 3 (a). The profiles were obtained along black-dashed lines in Fig. 2 (b) by assuming penetration depth of 6 μm and the sample density of 1.85 g/cm^3. Again, T concentration was clearly high at the center of the tile.

Pajuste et al. [13] examined T distributions on PFSs of the Be tiles after ILW-1 and ILW-2 by the dissolution in acid. In OPL, the T concentrations were higher than those in IWGL and DP. The T distribution on the PFS of OPL examined by Pajuste et al. [13] is plotted in Fig. 3 (b) with rhombus symbols indicating the highest concentration at the center. Our results are consistent with the observations of Pajuste et al. [13]. The distributions of D [4] and W [1] along toroidal direction on ILW-1 OPL are also plotted in Fig. 3 (b) with circle and triangle symbols, respectively. D and W showed opposite pattern to T and they are concentrated at the both sides of OPL. Similar profile to W was reported also for Ni [3,8].

The deposition of high atomic number elements such as Ni and W on Be reduces escape depth of β-rays from T. Nevertheless, the line profiles shown in Fig. 3 (a) are not significantly affected by the co-deposition of metal traces. This is because the concentration of W and Ni were almost flat in the distance around ± 70 mm from the center of OPL and sharply increased at the edges [1-3,8]. A clear change in the T concentration was observed within ± 70 mm from the center in Fig. 3 (a). In addition, the observed profiles were consistent with the results of dissolution measurements reported by Pajuste et al. [13], as previously mentioned.

The observed correlation between the distribution of D and that of metallic impurities shows that D was co-deposited with metallic elements. The thickness of deposition layer exceeded 10 mm at the left side edge of OPL [2]. Significantly different distribution of T from that of D and metallic impurities indicates T was retained in the tiles with different mechanisms; it is plausible that T was implanted into the tiles at high energy (1.01 MeV or lower values determined by energy loss in the plasma).

X-ray spectra obtained for castellation samples 127 (central part of OPL), 160 (edge of OPL) and 78 (DP) are given in Fig. 4 as typical examples. The intensity of the X-ray from sample 127 was far

higher than that from samples 160 and 78. This observation is consistent with IP results (Figs. 2 and 3). The sharp peak of Ar(Kα) characteristic X-rays and broad spectrum of bremsstrahlung were observed for all samples. The samples 160 and 78 also showed the peaks of characteristic X-rays of metallic impurities (Ni and W) due to deposition of these impurities. These results are also consistent with the observations in [1-3,8].

The characteristic X-rays of Ar are induced by β-rays from T within the escape depth of β-rays, while the bremsstrahlung is generated in the bulk of samples. Hence, intensity ratio between bremsstrahlung and Ar(Kα) line radiation, I_B/I_{Ar}, increases as penetration depth of T increases. This tendency is well reproduced by Monte Carlo simulation using toolkit Geant4 [14-17], as shown in Fig. 5 (a). In this figure, X-ray spectra obtained by simulation by assuming uniform penetration of T into Be up to 2, 4 and 6 μm are plotted. The increase in I_B/I_{Ar} with increasing T penetration depth is documented.

In Fig. 5 (b), the X-ray spectrum for sample 127 is compared with that obtained by simulation by assuming penetration depth of 6 μm. The simulated spectrum agrees well with the observed spectrum. Hence, it is concluded that the penetration depth of T in this sample is ~6 μm. Similar comparison for samples 13 and 78 has also shown a similar penetration depth of T.

In measurements performed by Pajuste et al. [13] the T concentration decreased with the increasing depth with smoothly falling tail (see Fig. 3 in [13]). The concentration reached a half of the maximum value at the depth of 4–5 μm. BIXS measurements provided a similar average penetration depth: a uniform T distribution up to a certain penetration depth. A dissolution method should provide more accurate result than BIXS if an ideal layer-by-layer etching is performed, but overestimation of T penetration depth is possible if the surface roughness is developed during etching due to a non-uniform dissolution rate.

The range of 1.01 MeV T ions in Be was evaluated using SRIM code [19] to be 10 mm at the normal incidence. T produced by DD reactions can be implanted into Be tiles at various incident angles. Hence, the penetration depth evaluated from BIXS spectrum (~6 mm) is consistent with the result of range calculation with SRIM code.

Fig. 6 shows T concentrations on PFSs of IWGL, OPL and DP after exposure to single (ILW-1, ILW-3) campaigns and during the entire operation period covering three campaigns: ILW-1,2,3. The value for each tile was evaluated for the location with the highest T concentration observed in the IP image by assuming that the T penetration depth is 6 □m and the density of sample is 1.85 g/cm^3. The T retention in OPL showed larger value after ILW-1,2,3 and ILW-3 than ILW-1. Similar tendency was observed also for IWGL. In contrast, the T retention in DP after ILW-3 showed smaller value than ILW-1.

The T retention in the erosion zones (the central parts of IWGL and OPL) is determined by implantation of high energy T (up to 1.01 MeV) and removal of T by erosion and/or thermal desorption. The amount of T produced by DD fusion reactions in ILW-3 should be larger than that in ILW-1 because of higher input power and longer discharge time (Table 2). The plasma interaction time with limiter tiles is summarized in Fig. 7 in [2]. The interaction time with IWGL and OPL was longer in ILW-1 than ILW-3. This means more erosion in ILW-1 than ILW-3. The larger T retention in OPL and IWGL after ILW-3 than ILW-1 can be ascribed to the combination of larger amount of T implantation and smaller extension of erosion. The T retention in DP cannot be simply correlated with the plasma interaction time. This is because DP received large amount of energy in disruptions [20] and the thermal desorption of T could be significant. According to Fig. 13 in [20], the number of disruption pulses delivering large amount of energy to DP2 (the second tile from the inboard side examined in this study) is larger in ILW-3 than ILW-1. This may be one of the causes of smaller T

retention observed for DP after ILW-3 than ILW-1. Information on disruption history in each experimental campaign and energy distributions on the DP tiles are necessary for more detailed discussion on T retention in DP.

3.2 Castellation grooves

The profiles of PSL intensity on castellation surfaces of samples 36, 78 and 127 are plotted against the distance from the entrance of the groove in Fig. 7, as typical examples. The PSL intensity had clear gradient for all cases and it decreased with increasing distance from the entrance. All four surfaces of the castellation were analyzed for each sample. No significant difference was observed between the surfaces parallel to the toroidal direction and those parallel to poloidal direction, thus confirming earlier data for deuterium obtained by ion beam analysis [9]. The PSL intensity in first 1–2 mm was sensitively dependent on the location in the tokamak. The highest PSL intensity was observed for sample 127 (the central part of OPL), which showed the highest T retention in PFS. Far lower PSL intensity was observed for the samples taken from the edge of OPL and those from IWGL and DP. Nonetheless, all castellation surfaces examined showed similar profiles in deeper region, i.e. the distance from the entrance larger than 2 mm, as shown in Fig. 7. D distributions on the castellation surfaces were examined by Rubel et al. [9]. The profiles of T shown in Fig. 7 were similar to those of D and metallic impurities in the deeper regions with the distance from the entrance larger than 2 mm. An agreement between the profiles of T, D and metallic impurities suggest that T and D are retained mainly by co-deposition with metallic impurities in the deep region of castellation grooves.

4. Conclusions

Distribution of T on PFSs and castellation grooves of Be limiter tiles retrieved from the main chamber of JET after ILW-1 and ILW-3 were examined using IP technique and BIXS. The observed T distributions on PFSs showed no systematic correlation with those of metallic impurities [1-4,8] and D [2-4]. The highest T concentration was observed at the center of OPL where the concentrations of D and metallic impurities showed the minimum values [1-4,8]. The T retention at this position was estimated to be 80 kBq/cm^2 after ILW-1 and 900-1000 kBq/cm^2 after ILW-3. The IWGL and DP showed orders-of-magnitude smaller T retention than OPL. In contrast, gradated distributions of T found at castellation grooves were similar to those of metallic impurities and D reported in [9]. These observations suggest T distributions on the PFSs were dominated by implantation of T at high energy, while those at the castellation grooves were controlled by co-deposition.

Acknowledgements

This work has been carried out within the framework of the EUROfusion Consortium and has received funding from the Euratom research and training programme 2014-2018 and 2019-2020 under grant agreement No 633053. The views and opinions expressed herein do not necessarily reflect those of the European Commission. The study was supported by JSPS KAKENHI (Grant no. JP26289353), the ITER Broader Approach Activities, and the National Institute for Fusion Research (NIFS) as a part of PWI Collaboration.

References

[1] A. Widdowson et al., Deposition of impurity metals during campaigns with the JET ITER-like Wall, Nuclear materials and Energy 19 (2019) 218-224. https://doi.org/10.1016/j.nme.2018.12.024.

[2] A. Widdowson et al., Fuel inventory and material migration of JET main chamber plasma facing components compared over three operational periods, Physica Scripta T171 (2020) 014051. https://doi.org/10.1088/1402-4896/ab5350.

[3] K. Heinola et al., Fuel retention in JET ITER-Like Wall from post-mortem analysis, Journal of Nuclear Materials 463 (2015) 961-965. https://doi.org/10.1016/j.jnucmat.2014.12.098.

[4] A. Baron-Wiechec et al., Thermal desorption spectrometry of beryllium plasma facing tiles exposed in the JET tokamak, Fusion Engineering and Design 133 (2018) 135-141. https://doi.org/10.1016/j.fusengdes.2018.05.075.

[5] A. Lahtinen et al., Deuterium retention in the divertor tiles of JET ITER-Like wall, Nuclear Materials and Energy 12 (2017) 655-661. https://doi.org/10.1016/j.nme.2017.04.007.

[6] J. Likonen et al., Investigation of deuterium trapping and release in the JET ITER-like wall divertor using TDS and TMAP, Nuclear Materials and Energy 19 (2019) 166-178. https://doi.org/10.1016/j.nme.2019.02.031.

[7] S. Brezinsek and JET-EFDA contributors, Plasma-surface interaction in the Be/W environment: Conclusions drawn from the JET-ILW for ITER, Journal of Nuclear Materials 463 (2015) 11-21. https://doi.org/10.1016/j.jnucmat.2014.12.007.

[8] A. Baron-Wiechec et al., Global erosion and deposition patterns in JET with the ITER-like wall, Journal of Nuclear Materials 463 (2015) 157-161. https://doi.org/10.1016/j.jnucmat.2015.01.038.

[9] M. Rubel et al., Fuel inventory and deposition in castellated structured in JET-ILW, Nuclear Fusion 57 (2017) 066027. https://doi.org/10.1088/1741-4326/aa6864.

[10] Y. Hatano et al., Tritium distributions on W-coated divertor tiles used in the third JET ITER-like wall campaign, Nuclear Materials and Energy 8 (2019) 258-261. https://doi.org/10.1016/j.nme.2019.01.001.

[11] Y. Hatano et al., Tritium analysis of divertor tiles used in JET ITER-like wall campaigns by means of β-ray induced x-ray spectrometry, Physica Scripta T170 (2017) 014014. https://doi.org/10.1088/1402-4896/aa8931.

[12] E. Pajuste et al., Structure, tritium depth profile and desorption from 'plasma-facing' beryllium materials of ITER-Like-Wall at JET, Nuclear Materials and Energy 12 (2017) 642-647. https://doi.org/10.1016/j.nme.2017.03.017.

[13] E. Pajuste et al., Comparison of the structure of the plasma-facing surface and tritium accumulation in beryllium tiles from JET ILW campaigns 2011-2012 and 2013-2014, Nuclear Materials and Energy 19 (2019) 131-136. https://doi.org/10.1016/j.nme.2019.02.011.

[14] S. Agostinelli et al., Geant4—a simulation toolkit, Nuclear Instruments and Methods in Physics Research Section A: Accelerators, Spectrometers, Detectors and Associated Equipment 506 (2003) 250-303. https://doi.org/10.1016/S0168-9002(03)01368-8.

[15] J. Allison et al., Geant4 Developments and Applications, IEEE Transactions on Nuclear Science 53 (2006) 270-278. https://doi.org/10.1109/TNS.2006.869826.

[16] J. Allison et al., Recent developments in Geant4, Nuclear Instruments and Methods in Physics Research Section A: Accelerators, Spectrometers, Detectors and Associated Equipment 835 (2016) 186-225. https://doi.org/10.1016/j.nima.2016.06.125.

[17] M. Röllig et al., Geant4 Monte Carlo simulations for sensitivity investigations of an experimental facility for the measurement of tritium surface contaminations by BIXS, Fusion Engineering and Design 109-111 (2016) 684-687. https://doi.org/10.1016/j.fusengdes.2016.02.018.

[18] EDS and low energy windows, https://www.amptek.com/products/sdd-x-ray-detectors-for-xrf-eds/eds-and-low-energy-windows/c-series-low-energy-x-ray-windows (current as of July 19, 2020).

[19] J. F. Ziegler, http://www.srim.org/ (current as of July 19, 2020).

[20] I. Jepu et al., Beryllium melting and erosion on the upper dump plates in JET during three ITER-like wall campaigns, Nucl. Fusion 59 (2019) 086009. https://doi.org/10.1088/1741-4326/ab2076.

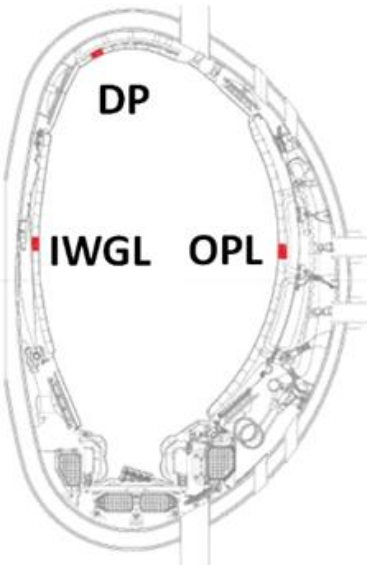

Fig. 1. Cross-sectional image of JET vacuum vessel and position of limiter tiles.

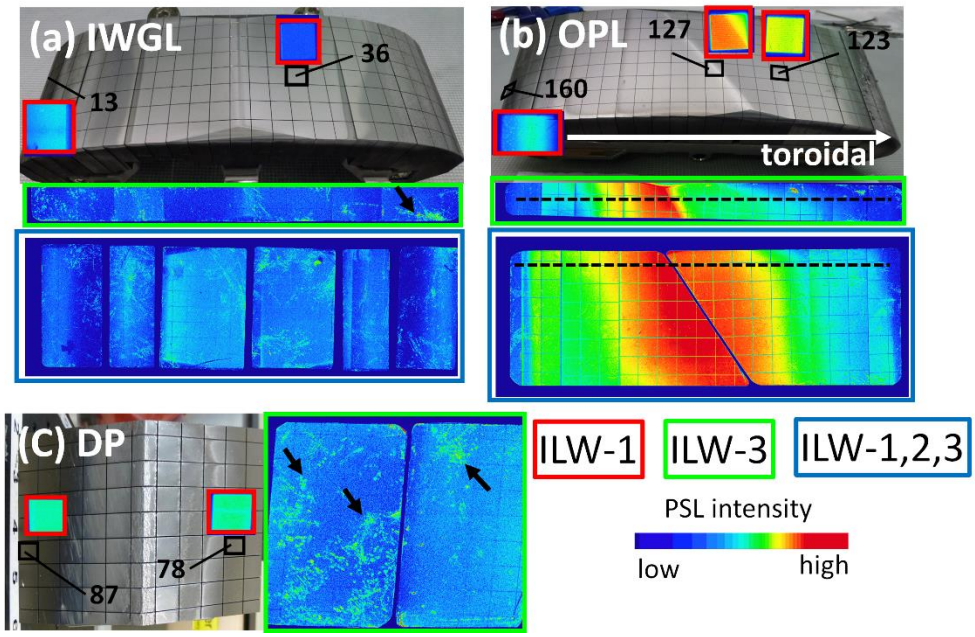

Fig. 2. Position of castellated samples and 2-dimensional distributions of photo-stimulated luminescence (PSL) intensity on the plasma-facing surfaces of Be limiter tiles obtained from IP measurements. A color scale from blue to red indicates the PSL intensity from the lowest to the highest. Line profiles shown in Fig. 3 are obtained from region indicated by black-dashed lines.

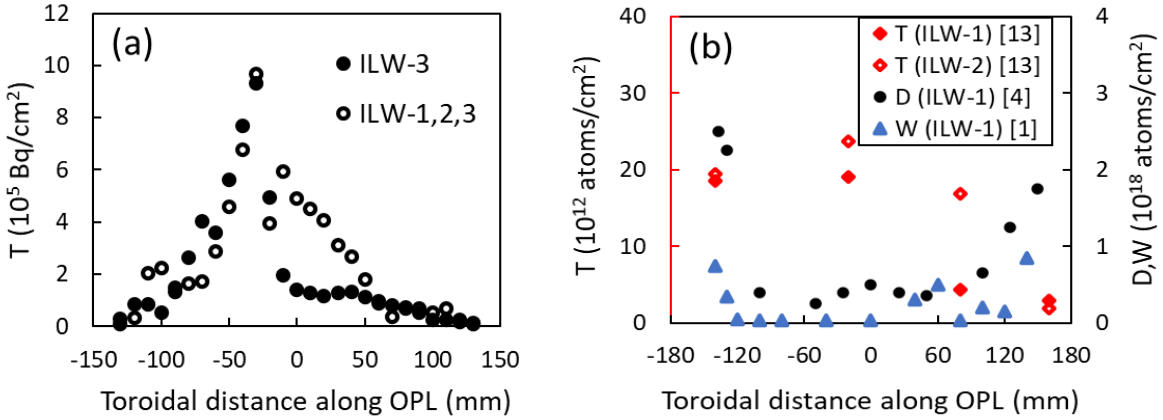

Fig. 3. T distribution along toroidal direction on plasma-facing surfaces of outer poloidal limiter (OPL) exposed to ILW-3 and ILW-1,2,3 (a) and that of T analyzed by acid dissolution method after ILW-1 and ILW-2 [13] together with distributions of D [4] and W [1] examined by ion beam analysis (IBA) (b). T retention in (a) was evaluated by assuming that T implantation depth is 6 μm.

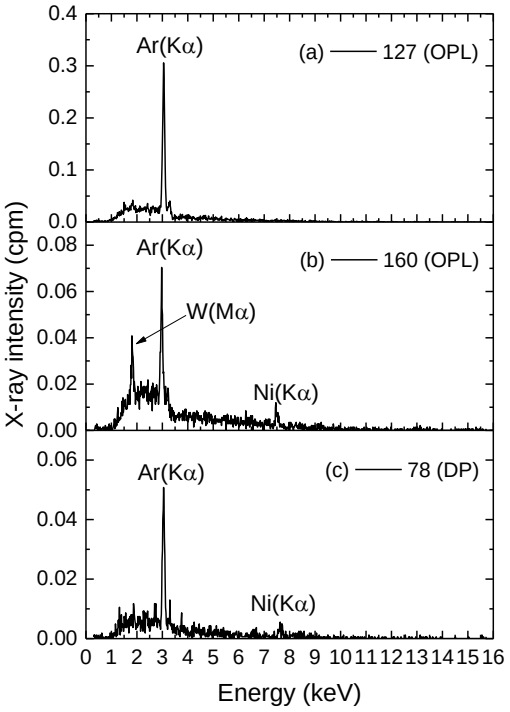

Fig. 4. Typical examples of X-ray spectra from castellation from Be limiter tiles retrieved after ILW-1: (a) 127 from OPL, (b) 160 from OPL and (c) 78 from DP (see Fig. 2)

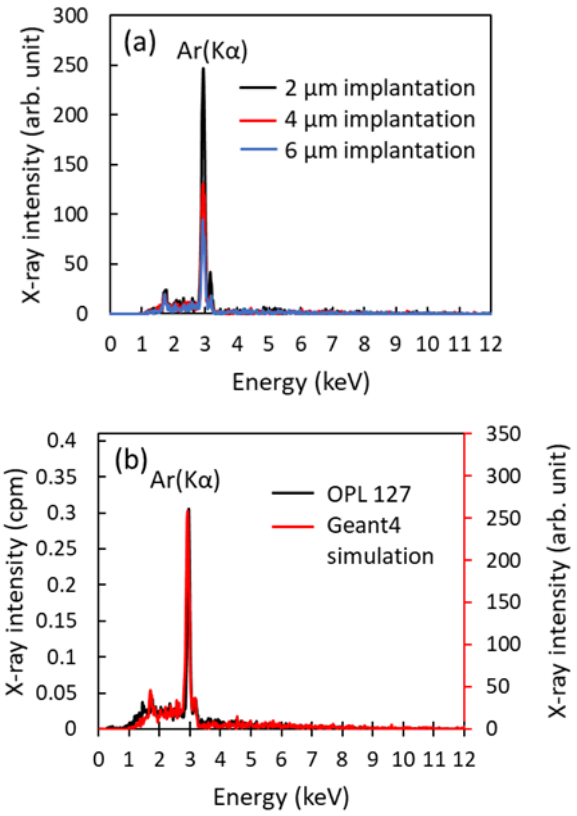

Fig. 5. (a) Results of Monte Carlo simulation using Geant4 by assuming uniform penetration of T up to 2, 4, 6 μm into Be layer, and (b) comparison of X-ray spectrum from sample 127 and that obtained by simulation by assuming T penetration of 6 μm.

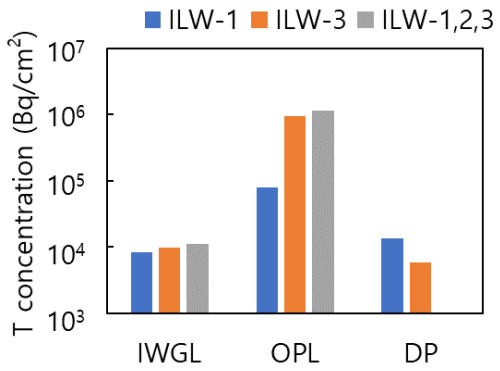

Fig. 6. Concentration of T evaluated from PSL intensity obtained by IP measurement. The regions with the highest PSL intensity were selected.

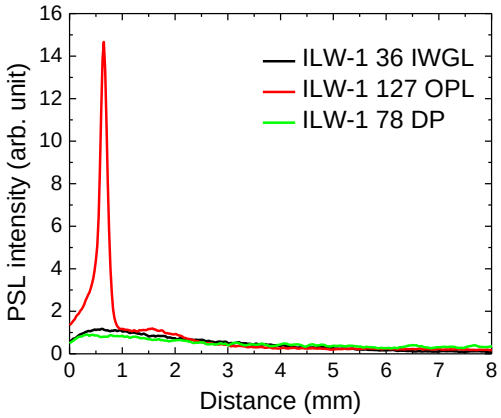

Fig. 7. Profiles of PSL intensity against distance from entrance of castellation groove. Castellation sample numbers are shown in the legend.

Table 1. Summary of Be limiter tiles and castellation samples from the tiles analyzed in this study. ILW-1,2,3 indicates tiles installed in JET for all three ILW campaigns.

Campaign	Limiter tiles	Castellation	Analysis
ILW-1	IWGL 2XR10	13, 36	IP, BIXS
	OPL 4D14	123, 127, 160	IP, BIXS
	DP 2BC2	78, 87	IP, BIXS
ILW-3	IWGL 2XR10	whole tile	IP
	OPL 4D14	whole tile	IP
	DP 2BC2	whole tile	IP
ILW-1,2,3	IWGL 2XR11	whole tile	IP
	OPL 4D15	whole tile	IP

Table 2. Operation parameters of ILW campaigns.

Parameter	**ILW-1**	**ILW-2**	**ILW-3**	**Total**
Total number of shots*	3668	4149	4420	12237
Total plasma time (h)	20.38	19.8	23.33	63.51
Limiter plasma (h)	7.76	6.04	4.86	18.66
Divertor plasma (h)	12.62	13.76	18.47	44.85
Input energy (GJ)	145	201	245	496
Fuel	D_2	Mostly D_2, Last 300 shots in H_2	D_2	